Tip-enhanced Raman scattering and near-field optical imaging of semiconducting monolayer and few-layer MoTe₂

B. Medini Rajapakse,^a Andrey V. Krayev,^{b,*} Luke N. Holtzman,^c Katayun Barmak,^c Paras N. Prasad,^{a,d} Luis Velarde^{a,d,*}

- ^a Department of Chemistry, University at Buffalo, SUNY, New York 14260, United States.
- ^b Horiba Instruments, Inc., Novato, California 94949, United States.
- ^c Department of Applied Physics and Applied Mathematics, Columbia University, New York, NY, 10027, United States.
- d The Institute for Lasers, Photonics and Biophotonics, University at Buffalo, SUNY, New York 14260, United States
- * Email: andrey.krayev@horiba.com and lvelarde@buffalo.edu

Abstract

Transition metal dichalcogenides (TMDs) offer exceptional platforms to study unique phenomena in two-dimensional (2D) materials. The understanding of phonon interactions in atomically thin TMDs is crucial for the development of novel applications. However, advancing our knowledge on phonon dynamics in TMDs under optical, thermal, electric, and strain perturbations requires comprehensive and minimally invasive chemical imaging techniques with nanoscale spatial resolution. Tip-enhanced Raman scattering (TERS) provides new promising avenues towards this goal while also enabling a detailed analysis of structural heterogeneity. Here, we demonstrate gap-mode TERS imaging of mechanically exfoliated monolayer and few-layer 2H-MoTe₂. At 633 nm, 671 nm, and 785 nm laser excitations, we report an overwhelmingly selective TERS enhancement of the out-of-plane A_{1g} phonon mode relative to in-plane E¹_{2g} phonon mode for mono- to few-layer MoTe₂. The pure near-field spectral line shapes are clearly distinct from the well-characterized far-field counterparts. We demonstrate that near-field interactions of selective phonon modes are extremely sensitive to the excitation wavelength, sample thickness, and structural defects. Our results therefore provide fundamental information for the nanoscale characterization of semiconducting MoTe₂-based devices.

1. Introduction

Two-dimensional van der Waals (vdW) materials with atomic-level thickness control can exhibit uniquely tailored properties, such as tunable optoelectronic phenomena and thickness-dependent charge carrier transport behavior. These tunable properties make them promising candidates for next-generation micro/nanoelectronics and ultrasensitive sensing platforms.[1-4] Transition metal dichalcogenides (TMDs), such as MoS₂, WS₂, MoSe₂ and

WSe₂, have been identified as semiconducting layered vdW materials that exhibit indirect-to-direct band gap crossover[5, 6] in single layers and continue to garner attention as emerging nanomaterials. Despite their exceptional properties, there are some inherent challenges for integrating such semiconducting materials into devices and systems, like computer chips, as their ultrathin structures can be susceptible to defects and nano- to micro-scale heterogeneity.[7] The ability for high-quality 2D materials to be transferred to a substrate for device fabrication and/or interface metrologies remains a challenge. Depending on the methodology used, various layer transfer processes may induce film deformation, damage, and introduce contaminants. Characterization methods that shed light on the structural properties of transferred 2D materials at the nanoscale are crucial for reassuring the reliability of the used approach. Minimally invasive methods for chemical imaging with atomic-level resolution offer the ability to determine if the 2D material has been subjected to strain and structural deformation on the target substrate and that interfaces are indeed pristine and free from defects. Tip-enhanced Raman scattering (TERS) and tip-enhanced photoluminescence (TEPL) are ideally suited for directly visualization of 2D semiconductors with nanometer-scale resolution.[8-12] Tip-enhanced spectroscopy overcomes the diffraction-limited spatial resolution via enhanced optical fields in proximity to an atomically sharp metallic tip.[13-16]

TERS is particularly useful for simultaneously investigating vibrational and optical properties of materials since the underlying factors governing the optoelectronic and thermal properties of these materials are strongly influenced by the spatio-temporal response of carriers and phonons toward external stimuli. A crucial step towards the application of 2D semiconductors is to understand how phonons may couple to plasmons and electrons, limit carrier mobility, and report on local heating and strain effects. Raman spectroscopy has been a remarkable tool to probe phonon dynamics[17, 18] and surface interactions,[19-21] and in the resonance regime, to gauge discerning factors concerning exciton-phonon coupling.[22-25] Most TERS studies are carried out in the "gap mode", where both the probe and the substrate are metallic (typically gold or silver) such that a plasmonic junction between the tip and the substrate is formed under illumination.[26, 27] The extreme localization and enhancement of the incident and scattered optical fields in this tip-substrate gap leads to a signal increase of 1–2 orders of magnitude compared to tip-only TERS from well-defined 2D crystals.[28]

In this work, we focus on TERS of mono- and few-layer 2H-MoTe₂ (hereby referred to as MoTe₂), an emerging TMD material with narrow indirect band gap around 1.0 eV in the bulk. This band gap is lower in comparison to other TMDs of the same family (such as MoS₂ and MoSe₂) and closer to indirect gap of silicon (1.1 eV). As a single-layer, MoTe₂ exhibits a direct bandgap of 1.1 eV, and therefore mono- and few-layer MoTe₂ has gained interest for applications in nano-optoelectronics[29-36] and as potential replacement and/or augmentation of silicon-based technologies.[37, 38] The exciton binding energy of multilayered MoTe₂ was found to be unusually large when compared with other multilayered TMD semiconductors.[39] Raman spectroscopy is commonly used for characterizing TMDs since it allows the correct determination of the number of layers at the atomic scale, including for MoTe₂.[40],[29],[41],[42, 43] Here, we present TERS measurements on mechanically exfoliated mono- and few-layer MoTe₂ carried out in the gap- mode using gold-coated AFM tips and substrates. For the excitation wavelengths used in our experiments (633 nm, 671 nm, and 785 nm), we observed layer-dependent spectra that are clearly different from their far-field counterparts. Selective enhancement of the out-of-plane MoTe₂ phonon mode (A_{1g}/A'_1) relative to the in-plane phonon mode (E^1_{2g}/E') at few-layer thickness was observed at all wavelengths, while expectedly, the near-field enhancement decreased with increased thickness. TERS enhancement and its mode-selectivity were found to depend on laser excitation wavelength, number of layers, and the presence of lattice deformation (strain) defects. Our findings demonstrate that the phonon modes of mono- to few-layer MoTe₂ are extremely sensitive to the electrical near-fields.

2. Experimental details

2.1 Sample preparation

High quality gold surfaces are typically used in TERS experiments to induce gap-mode TERS. In addition, it is known that the TMDs have strong affinity to bind to the gold surface and the so-called "gold-assisted" mechanical exfoliation has been used to obtain larger lateral size flakes with controlled thicknesses.[44-47] Our metallic substrates were prepared by depositing a 20 nm titanium adhesion layer followed by 60 nm gold onto clean 1 cm glass squares that were cut from a microscope slide. The deposition was done using an electron beam (e-beam) evaporator with glancing angle deposition (Kurt J. Lesker AXXIS). In our work, we use 60 nm e-beam deposited gold with roughness ~1 nm (see Fig. S1) to mechanically exfoliate 2H-MoTe₂ following the previously reported

TERS studies on TMDs, which is known to induce sufficient TERS enhancement.[10, 48] The gold coated substrates were then soaked in a solution of NOCHROMIX with concentrated sulfuric acid, thoroughly rinsed with ultrapure water (18.2 M Ω cm⁻¹), blow-dried with pure nitrogen gas and UV-ozone treated for 1 hour.

Crystals of 2H-MoTe₂ were grown at Columbia University via a two-step flux synthesis method that generates TMDs with high-purity and low defect density.[49] Flux synthesis has been reported to produce higher crystalline quality TMD single crystals than those produced by common commercial techniques such as chemical vapor transport. High-purity molybdenum powder (99.997%) and tellurium broken ingot (99.9999+%) were loaded into a quartz ampule, then sealed under vacuum and placed in a furnace. The furnace temperature was ramped to 1150°C over 36 hrs, then dwelled for two weeks, before cooling at 1°C/hr to 600°C. The cooling rate was increased to 5°C/hr until the temperature reached room temperature. The contents were then transferred to a second ampule with a quartz wool filter, sealed under vacuum, heated to 435°C, and flipped and centrifuged to extract MoTe₂ crystals from the excess tellurium. The MoTe₂ crystals were then annealed across a temperature gradient (T_{hot} = 435°C, T_{cold} = 25°C) for 48 hrs to remove any residual tellurium. The flux synthesis method resulted in TMD crystals with total defect densities less than 10¹² cm⁻² and the obtained crystals were 1-2 mm in lateral extension and ~500 μm thick.

A modified exfoliation method was used for transferring MoTe₂ onto the gold surface from the bulk crystals. This method was adapted from Huang et al. developed for exfoliation of graphene and expanded by other groups for TMDs.[50] In brief, the as-grown 2H-MoTe₂ is transferred to the thermally annealed (100°C for 20 minutes) flat target gold substrate using low-adhesion tape and was followed by a thermal annealing step at 100 °C for 5 minutes for generating larger area few-layer films. A subsequent controlled layer by layer oxidation method[51, 52] was used for obtaining larger area monolayer and few-layer MoTe₂ on gold.

2.2 Spectroscopy and microscopy methods

Micro-Raman measurements. A Horiba LabRAM HR 800 confocal Raman spectrometer was used for micro-Raman measurements using a 300 grooves/mm grating blazed for 600 nm and a 100X, 0.8 NA, objective. The laser output powers were kept in the 200 - 500 μW range. The Raman spectra were calibrated with respect to the silicon peak at 520.7 cm⁻¹.

Tip Enhanced Raman Scattering (TERS). TERS measurements of few-layer MoTe₂ were carried out in ambient conditions with an OmegaScope-R system (AIST-NT, Inc.; since 2017, HORIBA Scientific), coupled to the Horiba LabRAM HR confocal Raman spectrometer using a side-illumination geometry. Experiments were carried out with tips prepared by sputter coating 100 nm Au on silicon probes (ATEC-NC, Nano-sensors).[53, 54] Excitation wavelengths of 632.8 nm, 671 nm, and 785 nm were used with laser output power in the 200 - 500 μW range. Excitation and collection of scattered light was carried out using a 100X, 0.7 NA, long working distance objective and detected through a charge coupled device (CCD). The specific parameters and modes used for TERS mapping are specified in the results section. TERS signals were collected with the tip in contact on the surface with a force in the 5-10 nN range).

3. Results and discussions

Monolayer, few-layer and bulk MoTe₂ films on gold were initially identified using both optical contrast difference, as shown in optical images in Fig. 1(a), and AFM topographic analysis as displayed in Fig. 1(b). The height profile in Fig. 1(d) indicates the AFM thickness of regions with respect to the gold substrate level. Due to the roughness of the gold substrate being approximately ~1 nm, in addition to the topographic influence of surface interactions between the substrate and the sample, micro-Raman measurements of exfoliated MoTe₂ samples were carried out for confirming the number of MoTe₂ layers as shown in Fig. 1(c). Most of the previous micro-Raman studies have been carried out on MoTe₂ exfoliated on silicon or silica surfaces, with only a few reports of ultrathin MoTe₂ films on gold.[31, 35, 55] Bulk 2H-MoTe₂ belongs to the D_{6h} point group, with 18 normal vibrational modes of which 7 are Raman active (doubly degenerate in-plane E_{1g} , E^{1}_{2g} , E^{1}_{2g} and non-degenerate out-of-plane A_{1g}). There are optically inactive modes which may become active in few-layer MoTe₂, such as the non-degenerate out-of-plane B¹_{2g} mode (vide-infra). For few-layer MoTe₂, the point group symmetry varies for odd and even number of layers (D_{3d} and D_{3h}, respectively). E', E" and A'₁ labels are used for Raman active vibrational modes in odd-number-layered MoTe₂, while E_g and A_{1g} are used in even-layered structures. [56, 57] From here onwards, we will refer to vibrational modes according to the bulk notation (in-plane E^{1}_{2g} , out-of-plane A_{1g} and out-of-plane B^{1}_{2g}) to avoid confusion. The characteristic phonon modes of MoTe₂ in the 2H-phase are given by an out-of-plane vibration with A_{1g} symmetry around 170 cm⁻¹, an in-plane vibration with E_{2g} symmetry near 234 cm⁻¹, and an out-of-plane vibration with B¹_{2g}

symmetry at about 289 cm⁻¹. The Raman spectrum confirms a monolayer for the lower left region (labeled 1L) by the absence of the B^{1}_{2g} peak (inactive in a monolayer) and a stronger response of the A_{1g} mode relative to the E^{1}_{2g} mode particularly observed at 633 nm (1.96 eV) excitation wavelength, as previously reported on silica.[40, 58] The Raman spectrum for the upper right region was consistent with that of tri-layer MoTe₂ (labeled 3L) based on the relative intensities of A_{1g} and B^{1}_{2g} phonon modes (and also confirmed by the AFM height profile). The B^{1}_{2g} mode becomes Raman active in atomically thin MoTe₂ due to the translation symmetry breaking along the *c*-axis direction, and is therefore absent in both monolayer and bulk MoTe₂[42, 59] The striking difference of the Raman response from monolayer MoTe₂ in comparison to few layer MoTe₂ at 633 nm have been reported in previous experimental work as well, particularly the relative intensities of A_{1g} and E^{1}_{2g} modes. [40, 60-62]

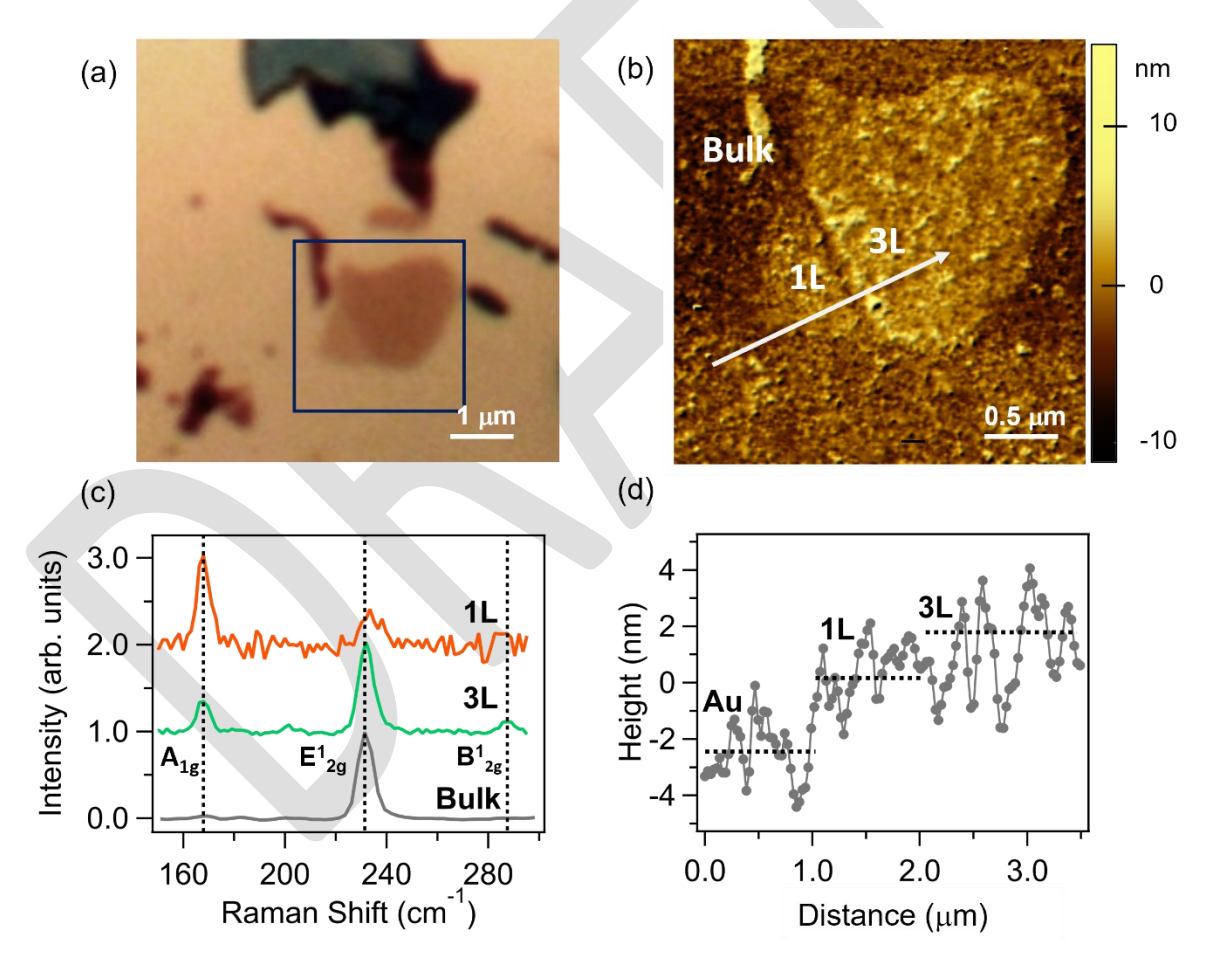


Fig. 1. Characterization of 2H-MoTe₂ monolayer (1L), tri-layer (3L) and multilayer (bulk) on gold. (a) Optical image of MoTe₂ exfoliated on e-beam gold with the boxed square marking the flake with monolayer (lower left zone) and tri-layer regions (upper right zone). (b) AFM topography from the selected square area in (a) representing regions with increasing thickness. (c) Micro-Raman spectra (background subtracted and normalized by the highest peak intensity) from regions corresponding to 1L, 3L and bulk regions illustrated in (b) It should be noted that Raman modes are labeled according to bulk notation. Height profile along white arrow in (b) is shown in (d) with dotted lines indicating the average step heights to trace the substrate (Au), 1L and 3L 2H-MoTe₂.

Our results show negligible differences in the Raman peak frequencies for MoTe₂ on gold in comparison to reports on SiO₂/Si substrates. The monolayer A_{1g} mode peak frequency on the gold substrate was 168.0 ± 0.6 cm⁻¹ and the E^{1}_{2g} mode was located at 233.4 ± 0.6 cm⁻¹. For the tri-layer, Raman peaks were observed at 168.4 cm ± 0.8 cm⁻¹ for the A_{1g} , 232.1 ± 0.2 cm⁻¹ for the E^{1}_{2g} , and 287.7 ± 0.2 cm⁻¹(B^{1}_{2g}). Davydov splitting of the A_{1g} mode has been reported at 633 nm for the tri-layer, [56, 63, 64] which becomes well resolved when using a 2400 grooves/mm grating (spectral resolution of ~ 0.4 cm⁻¹ per pixel).[56] Our spectral resolution with the 300 grooves/mm grating is approx. 2 cm⁻¹ per pixel at 633 nm and the peak width (full width at half maximum) of the A_{1g} peak at ~ 168 cm⁻¹ was ~ 4.0 cm⁻¹ which is not sufficient to resolve this splitting. A more in-depth analysis of the Davydov splitting is therefore out of the scope of the present study.

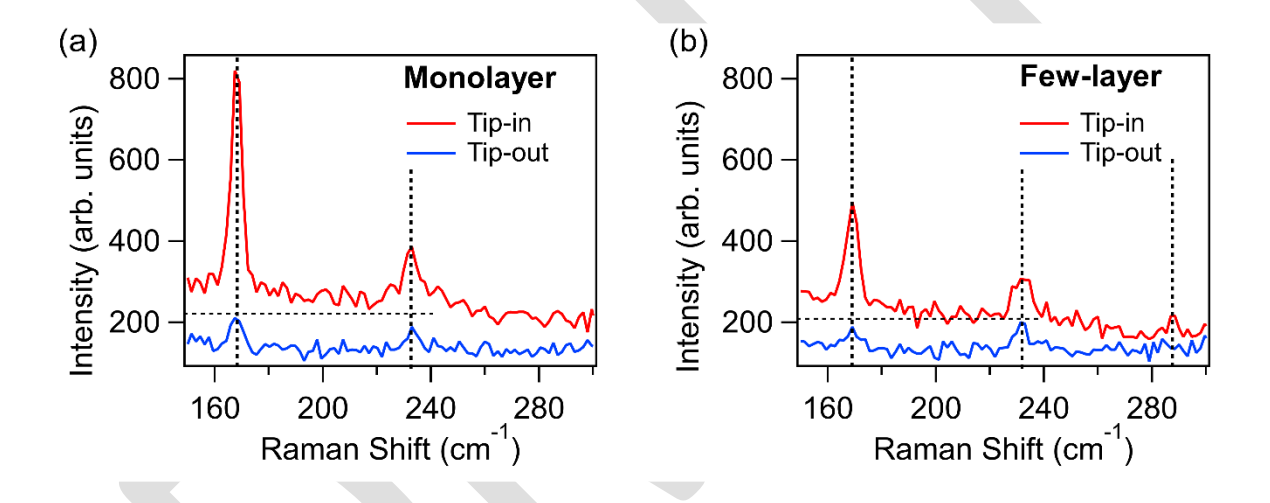


Fig. 2. TERS enhancement of the Raman signal for monolayer (1L) and few-layer (3L) MoTe₂ on gold substrate (shown in Fig. 1) observed with the tip in close proximity to the sample surface (tip-in, shown in red) compared to when the tip is away (tip-out, shown in blue). The excitation wavelength is 633 nm.

Fig. 2 shows point TERS measurements for the 1L and 3L MoTe₂ regions in Fig. 1 using 633 nm excitation. In both cases, we observed a significant difference in Raman spectral line shapes when the tip was brought in contact (tip-in), in comparison to when the tip is away from the material (tip-out), with approximate tip-sample distances of 0.5 nm and 20 nm, respectively. We particularly noticed that the A_{1g} mode at 168 cm⁻¹ has by far the strongest response in comparison to the E^{1}_{2g} mode at 234 cm⁻¹ (the most prominent peak of bulk MoTe₂). In other words, we show a selective enhancement of the out-of-plane A_{1g} phonon mode for mono- and few-layer MoTe₂ at the excitation

wavelength. This is consistent with a phonon mode with Raman tensor component along the z-direction (along the surface normal) according to the TERS selection rules. [65] Due to the side-illumination geometry used, the in-plane modes can be somewhat enhanced. To further evaluate this trend, we fitted the peaks to Lorentzian functions as shown in Fig. S3 in the Supporting Information and calculated near-field enhancement factors according to Zenobi and co-workers. [66] We observed that for the few-layer case, the A_{1g} mode is enhanced by a factor of 4×10^2 while the E^1_{2g} mode is enhanced by a factor of 0.6×10^2 . The enhancement factors for A_{1g} and E^1_{2g} modes in monolayer MoTe₂ are 7.1×10² and 1.4×10², respectively. In Fig. 2, we can see that while the far-field (FF) contributions (or tip-out) of the 1L and 3L regions are of comparable intensity (lower blue traces), the TERS enhancement of the A_{1g} mode is significant for both the 1L and 3L regions, with the monolayer showing larger enhancement compared with the few-layer region likely due to the increase of the gap-mode field enhancement with the decrease of the TMD flake thickness. [65] Fig. S4(A) in the SI shows that for thin few-layer samples (1.8 nm) in the gap-mode, the A_{1g} peak intensity for the tip-in spectrum surpasses the intensity of the E¹_{2g} mode, even if the FF (tip-out) contribution shows higher intensity in the E¹_{2g} in-plane mode. For 5.6 nm thick MoTe₂, the tip-in A_{1g} TERS enhancement is much weaker as shown in Fig. S4(B). Nonetheless, a preferential enhancement of the A_{1g} mode was still observable for the tip-in spectrum although the E¹_{2g} mode was now much higher in comparison. Fig. S5 shows the Raman spectra for multilayer (bulk) MoTe₂ (33.1 nm) for tip-in and tip-out conditions. The spectra show that at this thickness there was no measurable enhancement of any vibrational mode. This indicates that the TERS signal intensity decreases with increasing thickness for MoTe₂, as expected from the findings in previous studies of related 2D materials.[65, 67] It is important to notice, that while the appearance of the peak at 288 cm⁻¹ (B¹_{2g}) when tip is in contact with the material is evident for the few-layer region, it was not always clearly resolved in the tip-away spectrum; this is most likely due to low signal to noise ratios arising from the low laser power used during experiments. This phonon mode is inherently weaker in comparison to the E^{1}_{2g} mode, and the ratio between B^{1}_{2g}/E^{1}_{2g} has been commonly used for determination of layer thickness of MoTe₂[42] However, the rules for number of layer determination have not yet been established for near-field Raman.

Hyperspectral imaging in the Spec-Top mode (Horiba, AIST) was used to map intensities of the vibrational modes for tip-in and tip-out at each pixel generating two concurrent maps through which the pure near-field (PNF)

map can be obtained. To obtain the PNF contribution, the FF signal (tip-out) was subtracted from the tip-in TERS signals at each pixel. Topographic AFM image of a different MoTe₂ flake is shown in Fig. 3(a), with height profiles in Fig. 3(b) along the solid arrow shown in Fig. 3(a). The PNF map within the boxed red rectangular area of the AFM image is shown in Fig. 3(c), demonstrates clearly resolved step edges between the few-layer region and the multilayer zone. Fig. 3(d) shows the raw spectra averaged from areas indicated by the enclosed boxes X and Y in the corresponding PNF map. The selected area from the map corresponds to a sharp transition from few-layer MoTe₂ to bulk MoTe₂ respectively, with the red shading corresponding to the intensity of the A_{1g} peak. It is interesting to notice the difference in the PNF spectra in Fig. 3(d), in comparison to the FF micro-Raman spectra for few-layer (green trace in Fig. 1(c)) and bulk MoTe₂ (gray trace in Fig. 1(c)). When peaks are of similar intensities in both the tip-in and tip-out spectra, they cancel out and do not appear in the PNF spectrum. [68-70] Tip-in TERS enhancement of a particular mode would result in higher contribution to the PNF spectrum. Therefore, only the A_{1g} peak was used in the PNF maps since the other modes showed much weaker enhancement. The red color pixels in Fig. 3(c) indicate therefore the presence of few-layer MoTe₂. Although a pronounced layer difference is visible in the AFM topography image, the bulk region is not reflected in the PNF TERS map due to insignificant TERS enhancement at multilayer/bulk-like thicknesses (>10 nm), as shown in the PNF spectrum corresponding to boxed region Y. As expected, the PNF maps produce much sharper images of MoTe2 few-layer flakes compared to the FF counterparts (Fig. S6). It is also important to report that we did not observe a phase change from the semiconductor 2H phase to the metallic 1T phase under laser illumination during out TERS measurements due to heating or hot electron doping.[33, 70-72]

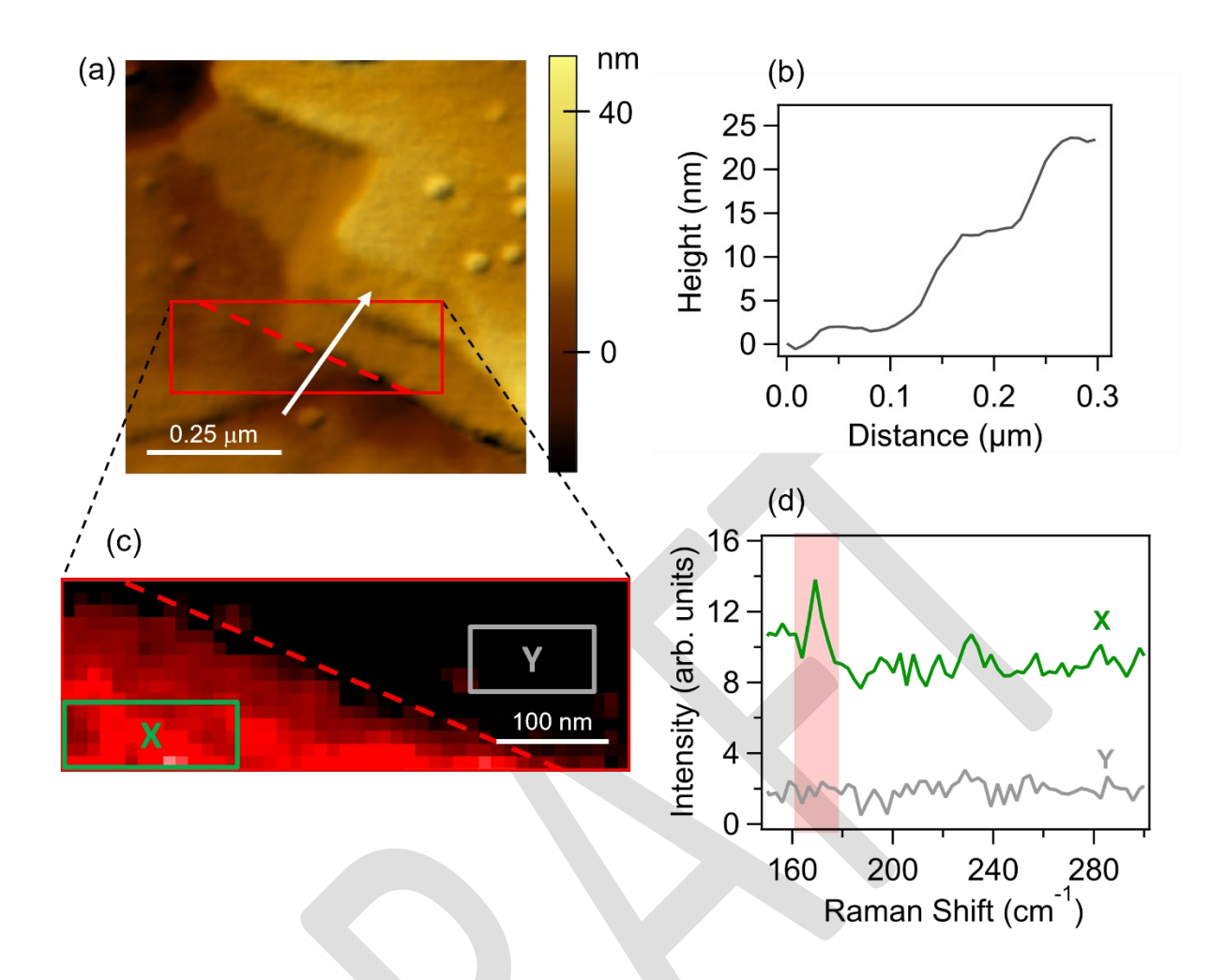


Fig. 3. (a) AFM topography of a MoTe₂ flake. (b) Height profile along the solid white arrow shown in (a), displaying average step heights of approximately 2 nm, 10.5 nm, and 11 nm along the arrow direction. (c) PNF TERS map of the A_{1g} mode peak area intensity for the boxed rectangular area in (a); the red dotted line (guide to the eye) follows along the interface between few-layer and multilayer (bulk) MoTe₂. (d) Averaged PNF TERS spectra from boxed areas X (few-layer) and Y (bulk), where the mapped the A_{1g} peak is highlighted in red. The excitation wavelength is 633 nm.

As reported in earlier studies, TERS measurements of TMDs at multiple wavelengths can reveal additional information about composition and exciton-phonon couplings.[73] Raman excitation with 632.8 nm light (1.96 eV) is known to resonantly enhance Raman scattering for the A_{1g} mode. This resonant behavior can be understood via electron-phonon couplings. The relative intensity of the A_{1g} mode to the E^{1}_{2g} mode in mono and few-layer MoTe₂ is significantly enhanced in the FF spectra because 1.96 eV is close to the energy of the A' (~1.73 eV) and B'(~2.0 eV) excitons.[40, 64] While the micro-Raman results at 632.8 nm reported a strong out-of-plane A_{1g} mode in comparison to the E^{1}_{2g} mode for 1L MoTe₂ that drastically weakened with increased crystal thickness, 785 nm excitation produced a much weaker E^{1}_{2g} response resulting in the A_{1g} mode being the strongest at all thicknesses.[57,

58, 63] The B¹_{2g} mode does not appear in the reported 785 nm Raman spectra for any crystal thickness. This has been explained on the basis of the laser excitation energy being far from the C exciton,[58] also assigned as the G-point direct gap.[39, 40, 74] The non-monotonic change of intensities in the resonant Raman scattering behavior in MoTe₂ has been rationalized in terms of both electron-phonon couplings and quantum interference effects.[41, 57, 62, 63]

To examine the effect of excitation photon energy, we carried out TERS measurements at 671 nm (1.85 eV) and 785 nm (1.58 eV). The PNF TERS spectra of few-layer MoTe₂ at these excitation wavelengths are shown in Fig. 4. In all 3 cases, the A_{1g} mode was the primary mode enhanced. The case of the out-of-plane E¹_{2g} peak at 234 cm⁻¹ and in-plane B¹_{2g} at 289 cm⁻¹ which were consistently low for all TERS measurements at 633 and 671 nm become negligible at 785 nm, indicating that the intensity of the A_{1g} mode is stronger in proximity of the A' and B' exciton region, while the E¹_{2g} shows modest enhancement at the lower excitation wavelengths likely at the energetic tail of higher energy excitons of different symmetry.[22, 39, 58]

PNF TERS mapping of few-layer MoTe₂ carried out at 785 nm excitation wavelength is shown in Fig. 5, focusing on a different MoTe₂ flake where nanoscale inhomogeneity was found in the sample (see Fig. S7 for the corresponding FF image). The AFM topographic image of the flake is shown in Fig. 5(a) with the height profile along the white solid arrow displayed in Fig. 5(b). The overall thickness of the flake is less than 4 nm. There are two regions with slightly different thicknesses separated by a 10 nm high structure. Contrary to the negligible enhancement for multilayer MoTe₂ as shown in Fig. 3(c)-(d), the higher TERS response characteristic of MoTe₂ suggest that this is likely due to lattice deformations caused by either a wrinkle[75, 76] or nano-protrusions in the gold substrate underneath the MoTe₂ sample,[48] and not due to the presence of a contaminant.

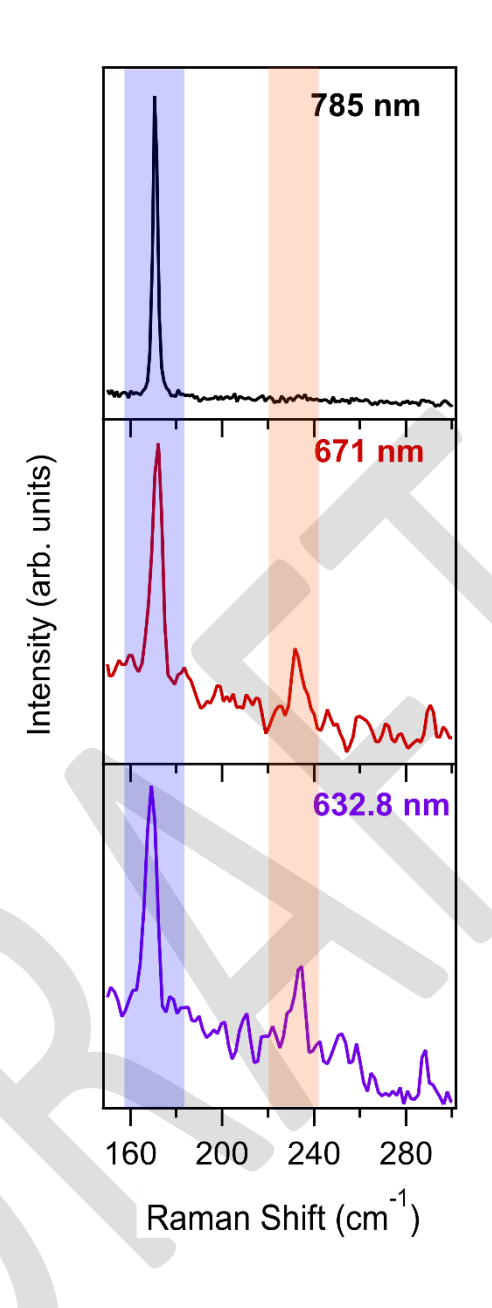


Fig. 4. Representative PNF TERS spectra of few-layer MoTe₂ (2-4 nm) with different excitation laser photon energies and normalized by the height of A_{1g} peak (blue shaded region).

In addition to the prominent A_{1g} mode at 170 cm⁻¹, which was already discussed in Fig. 4(a), we observed two other peaks appearing at ~234 cm⁻¹ and ~280 cm⁻¹ for the average of red boxes that were silent in the PNF spectra of the flat, pristine region of the flake. It is known that TMD wrinkles can increase TERS signals[75, 76] and deform the lattice so that otherwise exclusively in-plane modes may hold projections along the tip axis, which is a prerequisite for TERS.[75]

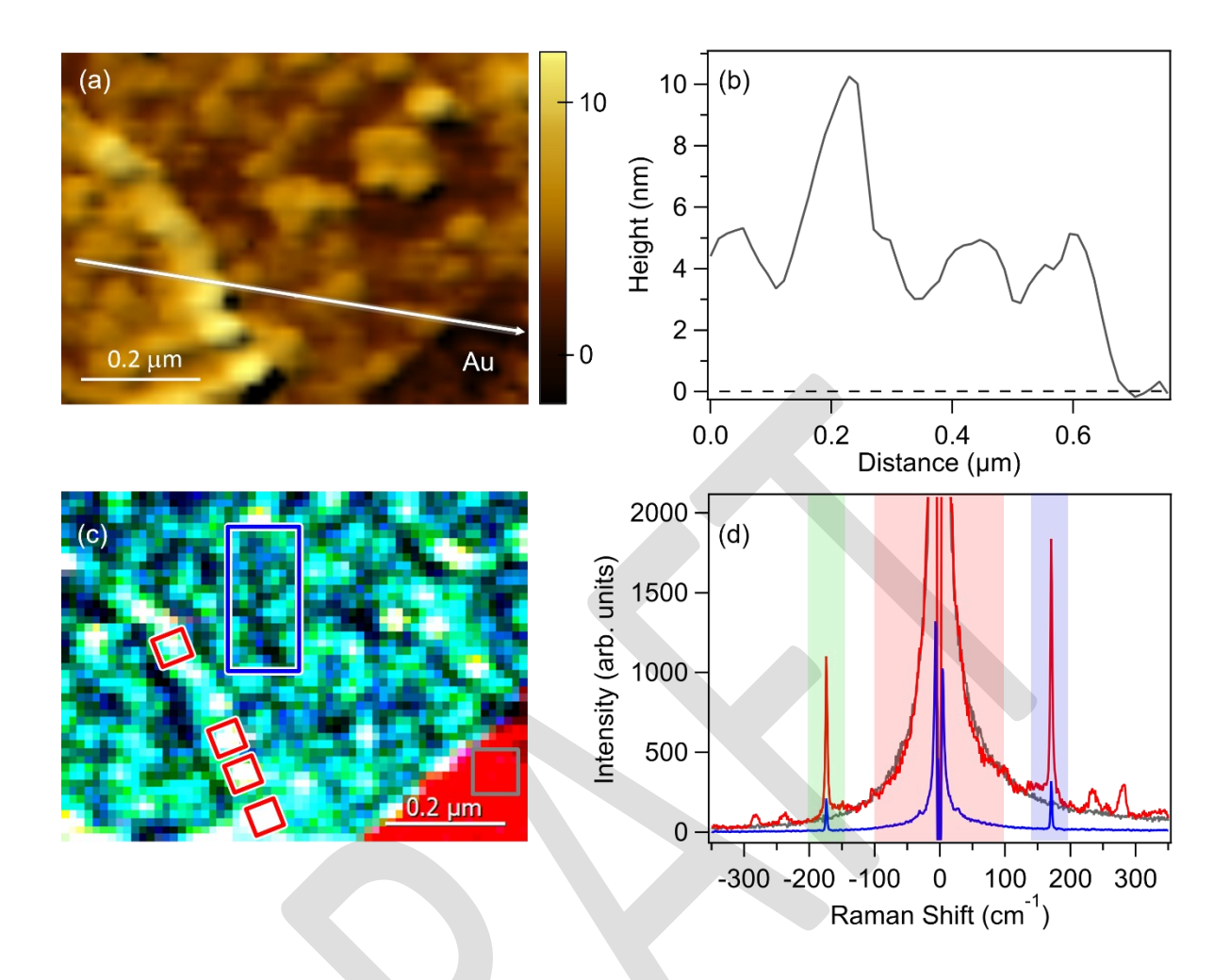


Fig. 5. PNF mapping at 785 nm (a) AFM topography of a MoTe₂ flake (Scale bar: $0.20 \,\mu\text{m}$), (b) Near-field TERS map showing the spatial distribution of correspondingly highlighted (Fig. 5(d)) spectral regions, including Stokes (blue), anti-Stokes (green), and the background near the Raman excitation line (red). (c) Height profile along the white arrow plotted in Fig. 5(a) (thickness of the whole flake area is ≤ 4 nm), (d) Averaged near-field spectra (including contributions from both stokes and anti-stokes Raman scattering regions) from the red boxes along the defect (red trace), the blue rectangular region (blue trace) and the grey box for the Au substrate (gray trace).

We would like to point out that the spectra in Fig. 5(d) show ultra-low frequency (ULF) modes below 60 cm⁻¹ are also TERS active as seen in Fig. 5(d). Interlayer oscillations are (i.e., shear and breathing modes)[77] related to layer displacements perpendicular and parallel to the *c* axis, respectively,[56, 61] the out-of-plane (breathing) mode c.a. 30 cm⁻¹ being more prominent here. Fig. S8 shows that the PNF spectra at frequencies below 100 cm⁻¹ are thickness dependent. A detailed study on ULF modes, however, is out of the scope of this work.

4. Conclusions

In summary, we report the first ever gap-mode TERS spectroscopy and imaging of 2H-MoTe₂, which are both sensitive to number of layers, excitation wavelength, and the presence of nanoscopic structural defects. The pure near-field TERS spectra unequivocally showed selective enhancement of the out-of-plane A_{1g} phonon mode relative to the in-plane E¹_{2g} phonon mode at mono- and few-layer thickness. This phenomenon was observed at all excitation wavelengths used in our experiments, namely 632.8, 671, and 785 nm, with the E¹_{2g} phonon mode weakening for the longer excitation wavelengths. Expectedly, the near-field enhancement decreased with increasing number of layers. The high spatial resolution of TERS imaging enabled clear distinction of step edges and nanosized structural defects for few-layer MoTe₂, which cannot be achieved using conventional micro-Raman spectroscopy. Our TERS experiments on mono- and few-layer MoTe₂ also shed light on near-field electron-phonon couplings with concurrent topographic imaging which is important for the development of MoTe₂-based nanotechnologies.

Declaration of competing interest

AVK is an employee of HORIBA Scientific, the manufacturer of the equipment used in this study. Collaboration with academia and industry is a part of his job responsibility.

Acknowledgements

BMR and LV gratefully acknowledge Chih-Feng Wang and Patrick El-Khoury from the Pacific Northwest National Laboratory for helpful discussions and providing gold coated tips. The authors thank Vasili Perebeinos at the University at Buffalo for helpful discussions. This work was supported by the Air Force Office of Scientific Research under award number FA9550-22-1-0312. LV acknowledges support from the National Science Foundation under the award number CHE-1900272. KB and LH acknowledge support under United States National Science Foundation Materials Research Science and Engineering Center DMR-2011738.

References

- [1] S.Z. Butler, S.M. Hollen, L. Cao, Y. Cui, J.A. Gupta, H.R. Gutiérrez, T.F. Heinz, S.S. Hong, J. Huang, A.F. Ismach, Progress, challenges, and opportunities in two-dimensional materials beyond graphene, ACS nano 7(4) (2013) 2898-2926.
- [2] D.L. Duong, S.J. Yun, Y.H. Lee, van der Waals layered materials: opportunities and challenges, ACS nano 11(12) (2017) 11803-11830.
- [3] D. Jariwala, V.K. Sangwan, L.J. Lauhon, T.J. Marks, M.C. Hersam, Emerging device applications for semiconducting two-dimensional transition metal dichalcogenides, ACS nano 8(2) (2014) 1102-1120.
- [4] O. Lopez-Sanchez, D. Lembke, M. Kayci, A. Radenovic, A. Kis, Ultrasensitive photodetectors based on monolayer MoS2, Nature nanotechnology 8(7) (2013) 497-501.
- [5] Y. Sun, D. Wang, Z. Shuai, Indirect-to-direct band gap crossover in few-layer transition metal dichalcogenides: a theoretical prediction, The Journal of Physical Chemistry C 120(38) (2016) 21866-21870.
- [6] I.G. Lezama, A. Arora, A. Ubaldini, C. Barreteau, E. Giannini, M. Potemski, A.F. Morpurgo, Indirect-to-direct band gap crossover in few-layer MoTe₂, Nano letters 15(4) (2015) 2336-2342.
- [7] P.F. Satterthwaite, W. Zhu, P. Jastrzebska-Perfect, M. Tang, S.O. Spector, H. Gao, H. Kitadai, A.-Y. Lu, Q. Tan, S.-Y. Tang, Y.-L. Chueh, C.-N. Kuo, C.S. Lue, J. Kong, X. Ling, F. Niroui, Van der Waals device integration beyond the limits of van der Waals forces using adhesive matrix transfer, Nature Electronics 7(1) (2024) 17-28.
- [8] K.-D. Park, O. Khatib, V. Kravtsov, G. Clark, X. Xu, M.B. Raschke, Hybrid tip-enhanced nanospectroscopy and nanoimaging of monolayer WSe₂ with local strain control, Nano letters 16(4) (2016) 2621-2627.
- [9] M. Velicky, A. Rodriguez, M. Bousa, A.V. Krayev, M. Vondracek, J. Honolka, M. Ahmadi, G.E. Donnelly, F. Huang, H.D. Abruna, Strain and charge doping fingerprints of the strong interaction between monolayer MoS₂ and gold, The journal of physical chemistry letters 11(15) (2020) 6112-6118.
- [10] K.K. Smithe, A.V. Krayev, C.S. Bailey, H.R. Lee, E. Yalon, B. Aslan, M. Muñoz Rojo, S. Krylyuk, P. Taheri, A.V. Davydov, Nanoscale heterogeneities in monolayer MoSe₂ revealed by correlated scanning probe microscopy and tip-enhanced Raman spectroscopy, ACS Applied Nano Materials 1(2) (2017) 572-579.
- [11] Y. Zhang, D.V. Voronine, S. Qiu, A.M. Sinyukov, M. Hamilton, Z. Liege, A.V. Sokolov, Z. Zhang, M.O. Scully, Improving resolution in quantum subnanometre-gap tip-enhanced Raman nanoimaging, Scientific reports 6(1) (2016) 25788.
- [12] J.F.S. A. Krayev, N. Jiang, S. Goswami, A. Tempez, S. Ambardar, D. V. Voronine, N. Kumar, K. Yao, S. Zhang, E. Yanev, K. McCreary, H-J Chuang, M. R. Rosenberger, T. Darlington, B. T. Jonker, J. C. Hone, D. N. Basov, P. J. Schuck, A. Patsha, Near-Field Nanospectroscopy and Tip-Enhanced Raman Spectroscopy (TERS), in: D.J. S. Dhara, S. Das (Ed.), Nanoscopy and Nanospectroscopy, CRC Press, Boca Raton, 2023, pp. 131-252.
- [13] R.M. Stöckle, Y.D. Suh, V. Deckert, R. Zenobi, Nanoscale chemical analysis by tip-enhanced Raman spectroscopy, Chemical Physics Letters 318(1-3) (2000) 131-136.
- [14] N. Hayazawa, Y. Inouye, Z. Sekkat, S. Kawata, Metallized tip amplification of near-field Raman scattering, Optics Communications 183(1-4) (2000) 333-336.
- [15] B. Pettinger, G. Picardi, R. Schuster, G. Ertl, Surface enhanced Raman spectroscopy: towards single molecule spectroscopy, Electrochemistry 68(12) (2000) 942-949.
- [16] M.S. Anderson, Locally enhanced Raman spectroscopy with an atomic force microscope, Applied Physics Letters 76(21) (2000) 3130-3132.
- [17] X. Lu, X. Luo, J. Zhang, S.Y. Quek, Q. Xiong, Lattice vibrations and Raman scattering in two-dimensional layered materials beyond graphene, Nano Research 9 (2016) 3559-3597.

- [18] X. Zhang, X.-F. Qiao, W. Shi, J.-B. Wu, D.-S. Jiang, P.-H. Tan, Phonon and Raman scattering of two-dimensional transition metal dichalcogenides from monolayer, multilayer to bulk material, Chemical Society Reviews 44(9) (2015) 2757-2785.
- [19] B. Breeman, A.T. Tiglias, J. Mancuso, E. Zurek, D.P. Miller, L. Velarde, Insight into the Adsorption Structure of TIPS-Pentacene on Noble Metal Surfaces, The Journal of Physical Chemistry C 126(5) (2022) 2689-2698.
- [20] S. Wood, J.R. Hollis, J.-S. Kim, Raman spectroscopy as an advanced structural nanoprobe for conjugated molecular semiconductors, Journal of Physics D: Applied Physics 50(7) (2017) 073001.
- [21] Y. Zhao, X. Liu, D.Y. Lei, Y. Chai, Effects of surface roughness of Ag thin films on surface-enhanced Raman spectroscopy of graphene: spatial nonlocality and physisorption strain, Nanoscale 6(3) (2014) 1311-1317.
- [22] B.R. Carvalho, L.M. Malard, J.M. Alves, C. Fantini, M.A. Pimenta, Symmetry-dependent exciton-phonon coupling in 2D and bulk MoS₂ observed by resonance Raman scattering, Physical review letters 114(13) (2015) 136403.
- [23] E. Del Corro, H. Terrones, A. Elias, C. Fantini, S. Feng, M.A. Nguyen, T.E. Mallouk, M. Terrones, M.A. Pimenta, Excited excitonic states in 1L, 2L, 3L, and bulk WSe₂ observed by resonant Raman spectroscopy, Acs Nano 8(9) (2014) 9629-9635.
- [24] P. Soubelet, A.E. Bruchhausen, A. Fainstein, K. Nogajewski, C. Faugeras, Resonance effects in the Raman scattering of monolayer and few-layer MoSe₂, Physical Review B 93(15) (2016) 155407.
- [25] J.-B. Wu, X. Zhang, M. Ijäs, W.-P. Han, X.-F. Qiao, X.-L. Li, D.-S. Jiang, A.C. Ferrari, P.-H. Tan, Resonant Raman spectroscopy of twisted multilayer graphene, Nature communications 5(1) (2014) 5309.
- [26] T. Deckert-Gaudig, V. Deckert, Nanoscale structural analysis using tip-enhanced Raman spectroscopy, Current opinion in chemical biology 15(5) (2011) 719-724.
- [27] J. Stadler, T. Schmid, R. Zenobi, Nanoscale chemical imaging using top-illumination tip-enhanced Raman spectroscopy, Nano letters 10(11) (2010) 4514-4520.
- [28] Z. Yang, J. Aizpurua, H. Xu, Electromagnetic field enhancement in TERS configurations, Journal of Raman Spectroscopy: An International Journal for Original Work in all Aspects of Raman Spectroscopy, Including Higher Order Processes, and also Brillouin and Rayleigh Scattering 40(10) (2009) 1343-1348.
- [29] N.R. Pradhan, D. Rhodes, S. Feng, Y. Xin, S. Memaran, B.-H. Moon, H. Terrones, M. Terrones, L. Balicas, Field-effect transistors based on few-layered α-MoTe₂, ACS nano 8(6) (2014) 5911-5920.
- [30] Y.F. Lin, Y. Xu, S.T. Wang, S.L. Li, M. Yamamoto, A. Aparecido-Ferreira, W. Li, H. Sun, S. Nakaharai, W.B. Jian, Ambipolar MoTe₂ transistors and their applications in logic circuits, Advanced Materials 26(20) (2014) 3263-3269.
- [31] X. Liu, A. Islam, N. Yang, B. Odhner, M.A. Tupta, J. Guo, P.X.-L. Feng, Atomic layer MoTe₂ field-effect transistors and monolithic logic circuits configured by scanning laser annealing, ACS nano 15(12) (2021) 19733-19742.
- [32] H. Luo, B. Wang, E. Wang, X. Wang, Y. Sun, K. Liu, High-responsivity photovoltaic photodetectors based on MoTe₂/MoSe₂ van der Waals heterojunctions, Crystals 9(6) (2019) 315.
- [33] Y. Wang, J. Xiao, H. Zhu, Y. Li, Y. Alsaid, K.Y. Fong, Y. Zhou, S. Wang, W. Shi, Y. Wang, Structural phase transition in monolayer MoTe₂ driven by electrostatic doping, Nature 550(7677) (2017) 487-491.
- [34] I.G. Lezama, A. Ubaldini, M. Longobardi, E. Giannini, C. Renner, A.B. Kuzmenko, A.F. Morpurgo, Surface transport and band gap structure of exfoliated 2H-MoTe₂ crystals, 2D Materials 1(2) (2014) 021002.
- [35] D. Qi, Q. Wang, C. Han, J. Jiang, Y. Zheng, W. Chen, W. Zhang, A.T.S. Wee, Reducing the Schottky barrier between few-layer MoTe₂ and gold, 2D Materials 4(4) (2017) 045016.
- [36] W. Zheng, M. Bonn, H.I. Wang, Photoconductivity multiplication in semiconducting few-layer MoTe₂, Nano letters 20(8) (2020) 5807-5813.

- [37] W. Hou, A. Azizimanesh, A. Sewaket, T. Peña, C. Watson, M. Liu, H. Askari, S.M. Wu, Strain-based room-temperature non-volatile MoTe₂ ferroelectric phase change transistor, Nature nanotechnology 14(7) (2019) 668-673.
- [38] A.M. Shafi, M.G. Uddin, X. Cui, F. Ali, F. Ahmed, M. Radwan, S. Das, N. Mehmood, Z. Sun, H. Lipsanen, Strain Engineering for Enhancing Carrier Mobility in MoTe₂ Field-Effect Transistors, Advanced Science 10(29) (2023) 2303437.
- [39] E. Jung, J.C. Park, Y.-S. Seo, J.-H. Kim, J. Hwang, Y.H. Lee, Unusually large exciton binding energy in multilayered 2H-MoTe₂, Scientific Reports 12(1) (2022) 4543.
- [40] C. Ruppert, B. Aslan, T.F. Heinz, Optical properties and band gap of single-and few-layer MoTe₂ crystals, Nano letters 14(11) (2014) 6231-6236.
- [41] H. Guo, T. Yang, M. Yamamoto, L. Zhou, R. Ishikawa, K. Ueno, K. Tsukagoshi, Z. Zhang, M.S. Dresselhaus, R. Saito, Double resonance Raman modes in monolayer and few-layer MoTe₂, Physical Review B 91(20) (2015) 205415.
- [42] M. Yamamoto, S.T. Wang, M. Ni, Y.-F. Lin, S.-L. Li, S. Aikawa, W.-B. Jian, K. Ueno, K. Wakabayashi, K. Tsukagoshi, Strong enhancement of Raman scattering from a bulk-inactive vibrational mode in few-layer MoTe₂, Acs Nano 8(4) (2014) 3895-3903.
- [43] R. Saito, Y. Tatsumi, S. Huang, X. Ling, M. Dresselhaus, Raman spectroscopy of transition metal dichalcogenides, Journal of Physics: Condensed Matter 28(35) (2016) 353002.
- [44] Y. Huang, Y.-H. Pan, R. Yang, L.-H. Bao, L. Meng, H.-L. Luo, Y.-Q. Cai, G.-D. Liu, W.-J. Zhao, Z. Zhou, L.-M. Wu, Z.-L. Zhu, M. Huang, L.-W. Liu, L. Liu, P. Cheng, K.-H. Wu, S.-B. Tian, C.-Z. Gu, Y.-G. Shi, Y.-F. Guo, Z.G. Cheng, J.-P. Hu, L. Zhao, G.-H. Yang, E. Sutter, P. Sutter, Y.-L. Wang, W. Ji, X.-J. Zhou, H.-J. Gao, Universal mechanical exfoliation of large-area 2D crystals, Nature Communications 11(1) (2020) 2453.
- [45] S.E. Panasci, E. Schilirò, G. Greco, M. Cannas, F.M. Gelardi, S. Agnello, F. Roccaforte, F. Giannazzo, Strain, Doping, and Electronic Transport of Large Area Monolayer MoS₂ Exfoliated on Gold and Transferred to an Insulating Substrate, ACS Applied Materials & Interfaces 13(26) (2021) 31248-31259.
- [46] E. Schilirò, S.E. Panasci, A.M. Mio, G. Nicotra, S. Agnello, B. Pecz, G.Z. Radnoczi, I. Deretzis, A. La Magna, F. Roccaforte, R. Lo Nigro, F. Giannazzo, Direct atomic layer deposition of ultra-thin Al2O3 and HfO2 films on gold-supported monolayer MoS₂, Applied Surface Science 630 (2023) 157476.
- [47] M. Velický, G.E. Donnelly, W.R. Hendren, S. McFarland, D. Scullion, W.J.I. DeBenedetti, G.C. Correa, Y. Han, A.J. Wain, M.A. Hines, D.A. Muller, K.S. Novoselov, H.D. Abruña, R.M. Bowman, E.J.G. Santos, F. Huang, Mechanism of Gold-Assisted Exfoliation of Centimeter-Sized Transition-Metal Dichalcogenide Monolayers, ACS Nano 12(10) (2018) 10463-10472.
- [48] W. Zhang, Cui, B.-S. Yeo, T. Schmid, C. Hafner, R. Zenobi, Nanoscale Roughness on Metal Surfaces Can Increase Tip-Enhanced Raman Scattering by an Order of Magnitude, Nano Letters 7(5) (2007) 1401-1405.
- [49] S. Liu, Y. Liu, L. Holtzman, B. Li, M. Holbrook, J. Pack, T. Taniguchi, K. Watanabe, C.R. Dean, A.N. Pasupathy, K. Barmak, D.A. Rhodes, J. Hone, Two-Step Flux Synthesis of Ultrapure Transition-Metal Dichalcogenides, ACS Nano 17(17) (2023) 16587-16596.
- [50] Y. Huang, E. Sutter, N.N. Shi, J. Zheng, T. Yang, D. Englund, H.-J. Gao, P. Sutter, Reliable exfoliation of large-area high-quality flakes of graphene and other two-dimensional materials, ACS nano 9(11) (2015) 10612-10620.
- [51] X. Zheng, Y. Wei, C. Deng, H. Huang, Y. Yu, G. Wang, G. Peng, Z. Zhu, Y. Zhang, T. Jiang, Controlled layer-by-layer oxidation of MoTe₂ via O₃ exposure, ACS applied materials & interfaces 10(36) (2018) 30045-30050.

- [52] A. Nipane, M.S. Choi, P.J. Sebastian, K. Yao, A. Borah, P. Deshmukh, Y. Jung, B. Kim, A. Rajendran, K.W. Kwock, Damage-free atomic layer etch of WSe₂: A platform for fabricating clean two-dimensional devices, ACS Applied Materials & Interfaces 13(1) (2020) 1930-1942.
- [53] A. Bhattarai, K.T. Crampton, A.G. Joly, L. Kovarik, W.P. Hess, P.Z. El-Khoury, Imaging the optical fields of functionalized silver nanowires through molecular TERS, The Journal of Physical Chemistry Letters 9(24) (2018) 7105-7109.
- [54] A. Bhattarai, B.T. O'Callahan, C.-F. Wang, S. Wang, P.Z. El-Khoury, Spatio-spectral characterization of multipolar plasmonic modes of Au nanorods via tip-enhanced Raman scattering, The Journal of Physical Chemistry Letters 11(8) (2020) 2870-2874.
- [55] N.J. Townsend, I. Amit, M.F. Craciun, S. Russo, Sub 20 meV Schottky barriers in metal/MoTe₂ junctions, 2D Materials 5(2) (2018) 025023.
- [56] G. Froehlicher, E. Lorchat, F. Fernique, C. Joshi, A. Molina-Sánchez, L. Wirtz, S. Berciaud, Unified description of the optical phonon modes in N-layer MoTe₂, Nano letters 15(10) (2015) 6481-6489.
- [57] M. Grzeszczyk, K. Gołasa, M. Molas, K. Nogajewski, M. Zinkiewicz, M. Potemski, A. Wysmołek, A. Babiński, Raman scattering from the bulk inactive out–of–plane B¹_{2g} mode in few–layer MoTe₂, Scientific Reports 8(1) (2018) 1-9.
- [58] B. Aslan, I.M. Datye, M.J. Mleczko, K. Sze Cheung, S. Krylyuk, A. Bruma, I. Kalish, A.V. Davydov, E. Pop, T.F. Heinz, Probing the optical properties and strain-tuning of ultrathin Mo_{1-x}W_xTe₂, Nano letters 18(4) (2018) 2485-2491.
- [59] S. Paul, S. Karak, A. Mathew, A. Ram, S. Saha, Electron-phonon and phonon-phonon anharmonic interactions in 2 H– MoX₂ (X=S, Te): A comprehensive resonant Raman study, Physical Review B 104(7) (2021) 075418.
- [60] K. Gołasa, M. Grzeszczyk, M.R. Molas, M. Zinkiewicz, K. Nogajewski, M. Potemski, A. Wysmołek, A. Babiński, Anomalous Raman scattering in few monolayer MoTe₂, MRS Advances 2(29) (2017) 1539-1544.
- [61] M. Grzeszczyk, K. Gołasa, M. Zinkiewicz, K. Nogajewski, M.R. Molas, M. Potemski, A. Wysmołek, A. Babiński, Raman scattering of few-layers MoTe₂, 2D Materials 3(2) (2016) 025010.
- [62] K. Gołasa, M. Grzeszczyk, M.R. Molas, M. Zinkiewicz, Ł. Bala, K. Nogajewski, M. Potemski, A. Wysmołek, A. Babiński, Resonant quenching of Raman scattering due to out-of-plane A_{1g}/A' ₁ modes in few-layer MoTe₂, Nanophotonics 6(6) (2017) 1281-1288.
- [63] H.P. Miranda, S. Reichardt, G. Froehlicher, A. Molina-Sánchez, S. Berciaud, L. Wirtz, Quantum interference effects in resonant Raman spectroscopy of single-and triple-layer MoTe₂ from first-principles, Nano Letters 17(4) (2017) 2381-2388.
- [64] Q. Song, Q. Tan, g.X. Zhang, J. Wu, B. Sheng, Y. Wan, X. Wang, L. Dai, P. Tan, Physical origin of Davydov splitting and resonant Raman spectroscopy of Davydov components in multilayer MoTe₂, Physical Review B 93(11) (2016) 115409.
- [65] D.V. Voronine, G. Lu, D. Zhu, A. Krayev, Tip-enhanced Raman scattering of MoS₂, IEEE Journal of Selected Topics in Quantum Electronics 23(1) (2016) 138-143.
- [66] J. Stadler, T. Schmid, R. Zenobi, Developments in and practical guidelines for tip-enhanced Raman spectroscopy, Nanoscale 4(6) (2012) 1856-1870.
- [67] A. Krayev, S. Krylyuk, R. Ilic, A.R. Hight Walker, A. Bhattarai, A.G. Joly, M.j. Velický, A.V. Davydov, P.Z. El-Khoury, Comparable enhancement of TERS signals from WSe₂ on chromium and gold, The Journal of Physical Chemistry C 124(16) (2020) 8971-8977.
- [68] B. Birmingham, Z. Liege, N. Larson, W. Lu, K.T. Park, H.W.H. Lee, D.V. Voronine, M.O. Scully, Z. Zhang, Probing interaction between individual submonolayer nanoislands and bulk MoS₂ using ambient TERS, The Journal of Physical Chemistry C 122(5) (2018) 2753-2760.

- [69] L.M. Malard, L. Lafeta, R.S. Cunha, R. Nadas, A. Gadelha, L.G. Cançado, A. Jorio, Studying 2D materials with advanced Raman spectroscopy: CARS, SRS and TERS, Physical Chemistry Chemical Physics 23(41) (2021) 23428-23444.
- [70] A.G. Milekhin, M. Rahaman, E.E. Rodyakina, A.V. Latyshev, V.M. Dzhagan, D.R. Zahn, Giant gapplasmon tip-enhanced Raman scattering of MoS₂ monolayers on Au nanocluster arrays, Nanoscale 10(6) (2018) 2755-2763.
- [71] Y. Tan, F. Luo, M. Zhu, X. Xu, Y. Ye, B. Li, G. Wang, W. Luo, X. Zheng, N. Wu, Controllable 2H-to-1T' phase transition in few-layer MoTe₂, Nanoscale 10(42) (2018) 19964-19971.
- [72] S. Cho, S. Kim, J.H. Kim, J. Zhao, J. Seok, D.H. Keum, J. Baik, D.-H. Choe, K.J. Chang, K. Suenaga, Phase patterning for ohmic homojunction contact in MoTe₂, Science 349(6248) (2015) 625-628.
- [73] A. Krayev, P. Chen, H. Terrones, X. Duan, Z. Zhang, X. Duan, Importance of Multiple Excitation Wavelengths for TERS Characterization of TMDCs and Their Vertical Heterostructures, The Journal of Physical Chemistry C 126(11) (2022) 5218-5223.
- [74] J.A. Wilson, A. Yoffe, The transition metal dichalcogenides discussion and interpretation of the observed optical, electrical and structural properties, Advances in Physics 18(73) (1969) 193-335.
- [75] A. Bhattarai, A. Krayev, A. Temiryazev, D. Evplov, K.T. Crampton, W.P. Hess, P.Z. El-Khoury, Tip-Enhanced Raman Scattering from Nanopatterned Graphene and Graphene Oxide, Nano Letters 18(6) (2018) 4029-4033.
- [76] R. Kato, T. Umakoshi, R.T. Sam, P. Verma, Probing nanoscale defects and wrinkles in MoS₂ by tipenhanced Raman spectroscopic imaging, Applied Physics Letters 114(7) (2019).
- [77] L. Liang, J. Zhang, B.G. Sumpter, Q.-H. Tan, P.-H. Tan, V. Meunier, Low-Frequency Shear and Layer-Breathing Modes in Raman Scattering of Two-Dimensional Materials, ACS Nano 11(12) (2017) 11777-11802.